JAHRBUCH DER GEOLOGISCHEN BUNDESANSTALT
Jb. Geol. B.-A. | ISSN 0016-7800 | Band 139 | Heft 2 | S. 215-232 | Wien, August 1996

Wrenching of a Continental Lithosphere Containing a Circular Resistant Inclusion: Physical Model Experiments

PETR RAJLICH, MIROSLAV BENES & PETER R. COBBOLD*)

19 Text-Figures

Böhmische Masse
Bruchtektonik
Rheologie
Experimentelle Tektonik
Lithosphäre

Contents

Blattverschiebungsmuster einer kontinentalen Lithosphäre in Anwesenheit eines runden, rigiden Körpers: Physikalische Modellversuche

Zusammenfassung

Ein Bruchnetzmuster, das in einer durch Blattverschiebung deformierten heterogenen Lithosphäre um einen harten Körper gebildet wurde, weicht von der homogen Lithosphäre ab in

1) vorzeitiger und bevorzugter Lokalisierung der Brüche um den harten Körper,
2) komplexer transtensionaler und transpressionaler drehender Kinematik der Blattverschiebungen um den harten Körper und in
3) der rautenförmigen Anordnung der den harten Körper umrahmenden Brüche.

Diese Strukturen tauchen in analogen physikalischen Modellversuchen auf, die eine laminierte Lithosphäre simulierten, zusammengesetzt aus duktilen und spröden Lagen, die durch gegenläufige Kräfte deformiert wurde. Die auch in Bezug auf die Gravitationsverhältnisse maßstabgerechten Modellversuche enthüllen Grundgesetze der Lithosphärendeformation in Anwesenheit runder, rigider Körper. Die Brüche umrahmen in invertierter Scherung vollkommen die Kreisstruktur. Dieses Modell erklärt am besten die Großstrukturen der Böhmischen Masse.

*) Authors' Addresses: PETR RAJLICH: Neústupného 1838, 155 00 Prague 515, Czech Republic; MIROSLAV BENES: Marine Geology Research Laboratory, University of Toronto, Department of Geology, Earth Sciences Centre, 22 Russell Street, Toronto, Ontario, M5S 3B1, Canada; PETER R. COBBOLD: Géosciences Rennes, UPR 4661 CNRS, University of Rennes I, Campus de Beaulieu, 35042 Rennes Cedex, France.

Abstract

A fault pattern induced by a stiffened body in a wrenched heterogeneous continental lithosphere plate differs from the homogeneous plate in
1) premature and preferential localization of fractures around the resistant structures,
2) complex transtensional and transpressional pivoting kinematics of mimetic faults around the rigid body and
3) lozenge-like geometry of the block surrounding the unyielding body.

These structures appear in analogical physical models of lithosphere deformed in forward and backward wrenching and composed of brittle and ductile layers. The models scaled for gravity reveal the possible basic behavior of the lithosphere in presence of rigid circular structures. Inverted shearing faults completely contour the circular structure. This model adapts best to the Bohemian Massif.

1. Introduction

Isolated structures with a resistant behavior are often found in the interior or on the borders of the collisional mountain belts (ZIEGLER, 1990). They carry different names in the geological literature such as Zwischengebirge (KOSSMAT, 1927), median mass (SCHTCHEGLOV, 1971), promontories (WILLIAMS, 1978), blocks (COBBOLD et al., 1993). They manifest generally relatively lower or no deformation during the collision (VILOTTE et al., 1984; ENGLAND & HOUSEMAN, 1985) that propagate in the rigid and plastic style inside the continental plate. Analogous examples feature geological maps of Australia, Northern America (WILLIAMS, 1978) and Central Asia (GALAGHER, 1981), Siberia (POROSHIN, 1981), Africa (HOLMES, 1967). These structures may have originated in different processes. Ocean floor accreted during the continental collision; the blocks with the particular thermal history (MOLNAR & TAPONNIER, 1981) or circular failures intruded by the maphic rocks may represent likely possibilities. Many have the circular form of the consistent radius (SAOUL, 1978; NORMAN, 1984) and display circular patterns of the Earth's surface. Generations of geologists since SUESS (1885, 1888, 1901, 1909) discussed in the Bohemian Massif the departure from the smooth general trend of the alpine mountain belt in Central Europe (Text-Fig. 1 and 2). Located in the orogenic belt, borders of these blocks are frequently the sites of an intense fracturing and create a particular fault grid as it is visible on the Bohemian Massif in Central Europe or Colorado Plateau (R. KRANTZ, oral communication). We present here experimental models of deformation of the lithosphere including these structures.

2. Physical Modelling

We performed the physical modelling in order to perceive the behavior of resistant isometric-circular bodies in a wrenching lithosphere and trace the progressive growth and pattern of the surrounding faults. We planned the models for the comparison between the demeanor and lack of rigid bodies of lithospheric dimensions, for the presence of two bodies and for the variable thermal conditions of the lithosphere layering, presuming cold (Archean) 4 rheological layers and hotter (late Variscan) 3-layers lithosphere (RANALLI & MURPHY, 1987).

The experiments have shown that substantial contrasts exist in fracture propagation, the inner rotation of blocks and history of deformation between homogeneous plates and plates with rigid heterogeneity. Dimensions and the fault pattern of the stiffened structure of the Bohemian Massif (Text-Fig. 1 and 2) served for the quantitative (displacement) and qualitative (sense of the displacement, fracturing style, fault network) design of the model. The models are thus comparable with the real geological situation in the field. The other interest is the possibility to study and predict the deformation in the deeper parts of the lithosphere. Combined information collected from topography, ductile deformed metamorphic levels and from geophysical surveying can be compared with the physical modelling.

2.1. Experimental Apparatus

Simple shear boxes inserted in the large container filled up with the honey represented the experimental device (Text-Fig. 3).

Moving facing solid walls of the shear box (Text-Fig. 3A and B) simulated the shear zone. In order to permit the stretching of the two rotating walls, we have built them from the gum sheets. The length of the stretched part of walls modelled the size of the shear zone inside the larger homogeneous plate (Text-Fig. 9). The computer driven screw jack enabled the mobile wall to move 18 cm forward and backward providing shear strains of the maximal amplitude of 0.29, 0.6 and 1.8 γ.

2.2. Model Materials and Scaling

Accepting that the upper crust obeys a MOHR-COULOMB yield criterion where strength increases with depth, we used dry quartz sand of a small cohesive force with a grain size about 400 μm and an angle of internal friction about 30–40° (KRANTZ, 1991). Admixture of ethyl cellulose powder reduced its density down to 1.2. Supposing further an average effective viscosity of the ductile lower crust to be about 10^{20} Pa s, we modelled it using Silbione silicone putty that has the perfect property of the Newtonian fluid with a viscosity of about 10^4 Pa s and density of 1.2 g cm^{-3}. The viscosity ratio was therefore 10^{16}. For the lithosphere mantle we used a mixture of Silbione putty and powdered galena, with a viscosity of 10^5 Pa s and a density of 1.4 g cm^{-3}.

The product of the length and density ratio provides the strength ratio (VENDEVILLE, 1987; DAVY, 1988; DAVY, 1991; COBBOLD, JACKSON, 1992; COBBOLD et al., 1993). We choose a density ratio of 2.5 in order to scale the strength ratio of the model in a normal gravity field (see Appendix). The chosen density ratio 2.5 corresponds to strength ratio of 1.8×10^6. The scaling obtained is 1:2 with 1 cm corresponding to 20 km in the vertical section and to 20 km in the horizontal distance. The ensued thickness of the sand layer of the "upper brittle crust" is 8 millimeters, the silicone of the "ductile crust" 10 millimeters, the thickness of the sand of the "brittle mantle" was 4 and the silicone of the "ductile mantle" 10 millimeters. Additional 4 millimeters of the sand stiffened the circular body and depressed correspondingly the ductile crust (Text-Fig. 3).

The scaled speed of the piston was 6 cm per hour for the large lithosphere and 14 cm for the narrow shear zone. This had for result more localized (slower speed of piston) or more distributed (quicker speed) fracturing. The models

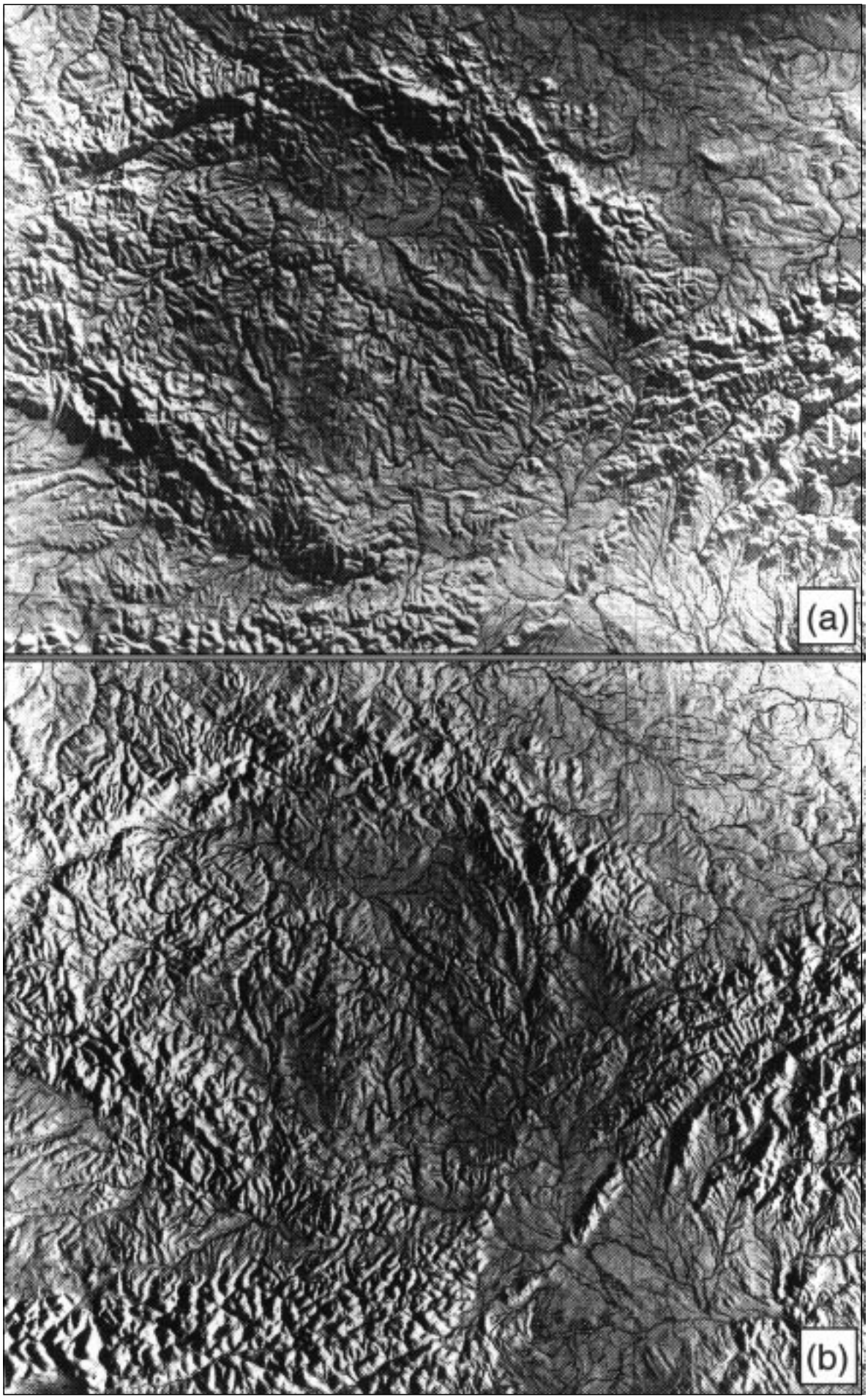

Text-Fig. 1. Plastic relief map of the Bohemian Massif illuminated from NE (a) and SE (b).

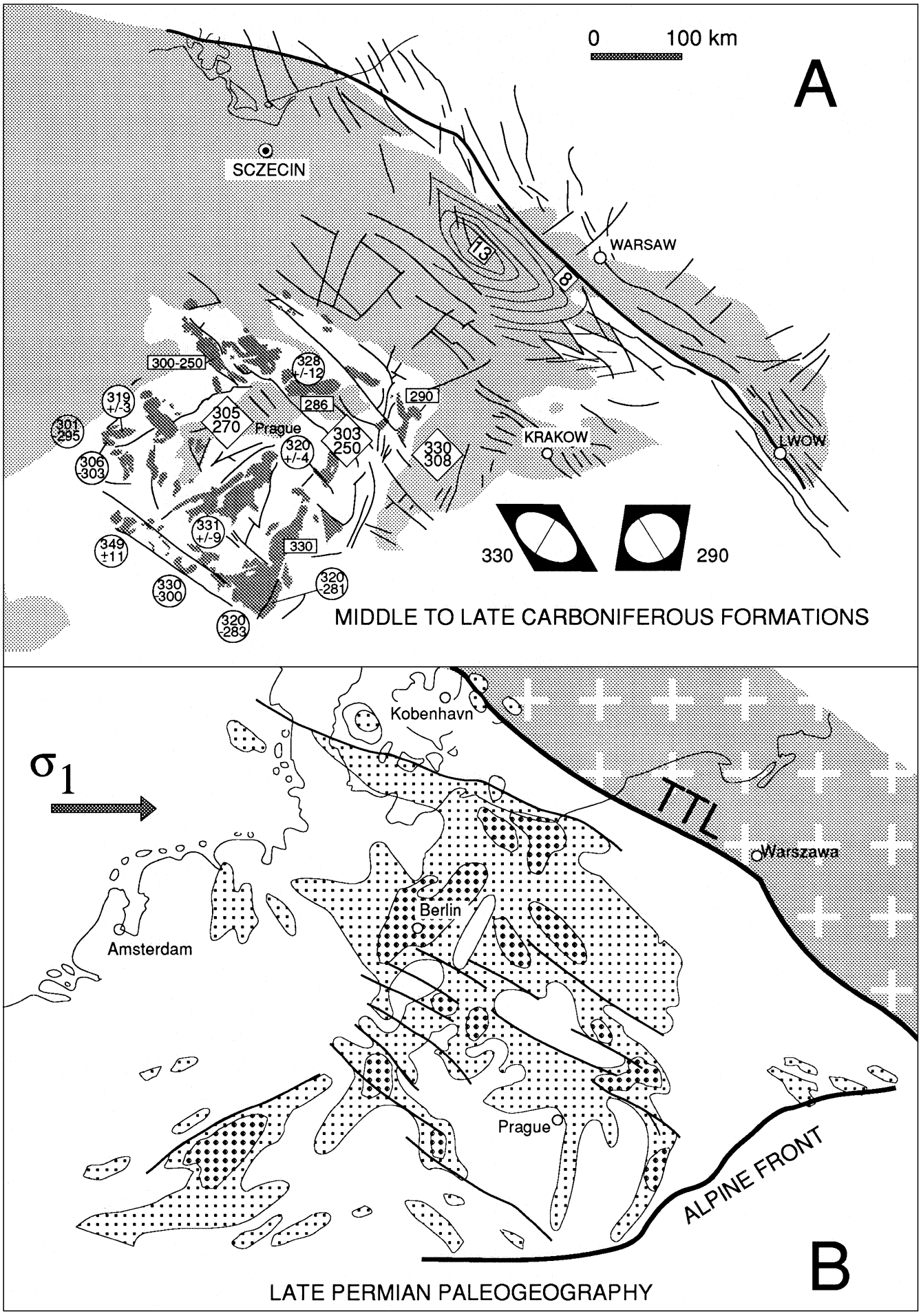
0 100 km
A
SCZECIN
WARSAW
KRAKOW
LWOW
Prague
13
8
300-250
328
+/-12
319
+/-3
286
290
305
270
303
250
320
+/-4
330
308
301
295
306
303
331
+/-9
330
349
+11
330
300
320
281
320
283
330
290
MIDDLE TO LATE CARBONIFEROUS FORMATIONS
σ1
Kobenhavn
TTL
Warszawa
Amsterdam
Berlin
Prague
ALPINE FRONT
B
LATE PERMIAN PALEOGEOGRAPHY

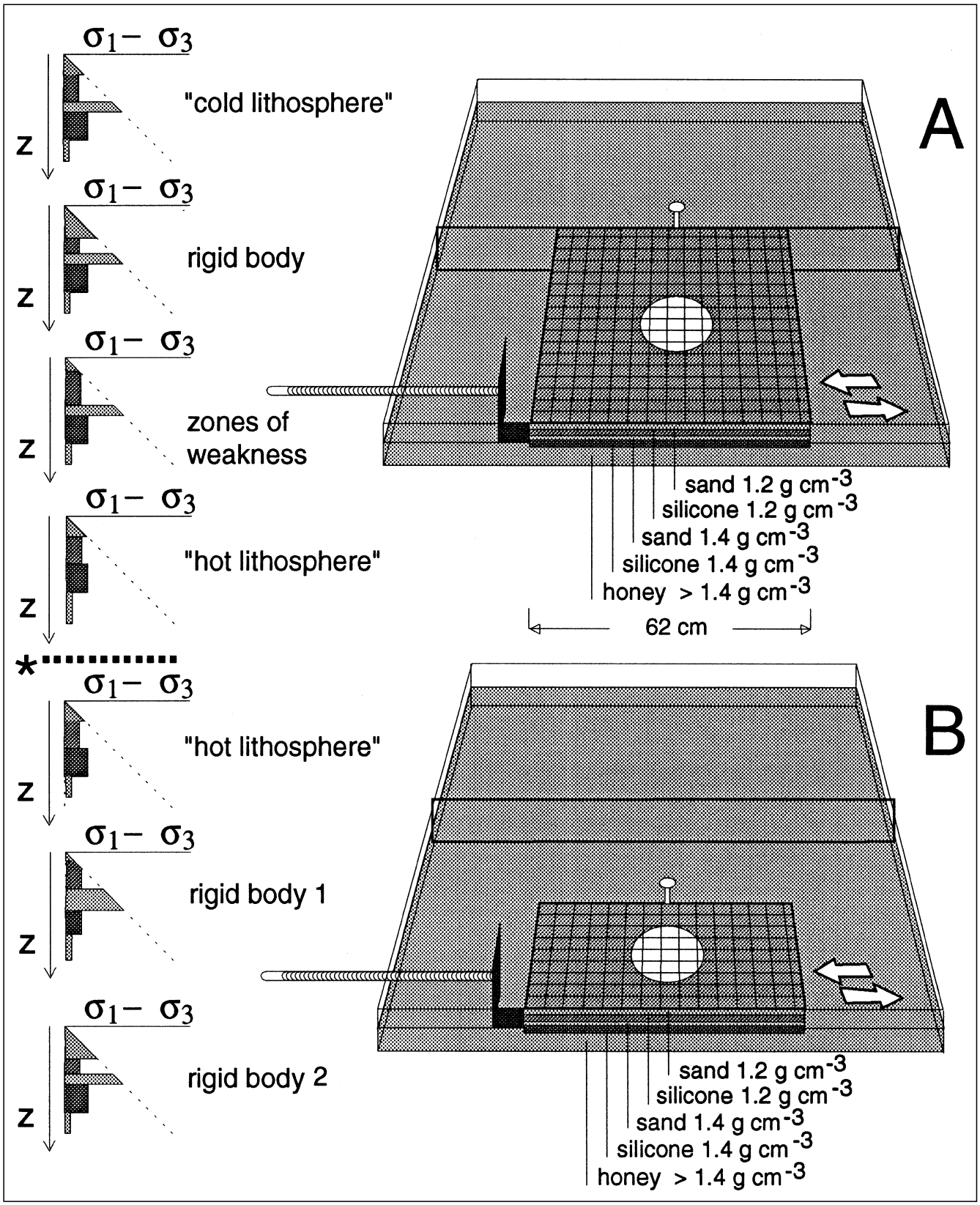

Text-Fig. 2. ◀ ◁ ◀
Behavior of the stiffened circular structure of the Bohemian Massif in orogenies.
A) Paleogeography and granites of the Upper Carboniferous; data in circles: Rb-Sr dating; squares: ages of sedimentary units; rectangles: Ar/Ar. Data from VACEK et al. (1988); TTL: TORNQUIST-TEISSEYRE line.
B) Permian palaeogeography and faults (BENEK, 1988), modified; degree of shadowing corresponds to the depth of the Autunian <1000 m and >1000 m.

Text-Fig. 3. ▲ △ ▲
Experimental device and rheology profiles employed in the experiments (see Appendix).
A) large shear zone scene.
B) narrow shear zone.
Different ratios of sand (brittle layers: clear grey shadowing – rhomboids) and silicone (ductile layers: dark grey shadowing – rectangles) employed in the experiments come into view on the left side of the Text-Figure.

were isothermal, without mechanical effects of thermal readjustments. They thus represent rapid tectonic deformation. We deformed the assembled models in the shear box enclosed in tanks filled up with the honey of the density of 1.5 g cm^{-3}.

The dimensions of the model (62 x 62 cm for the large lithosphere and 60 x 35 cm for the narrow lithosphere zone) were in this first approach patterned in agreement with the size of the Bohemian Massif and its surroundings:

1) distance to the TORNQUIST line and to the Variscan Alps on the South.
2) Zone of influence of the Permian subsidence and faulting (Text-Fig. 1 and 2).

The diameter of the rigid body in models was 14 cm (280 km).

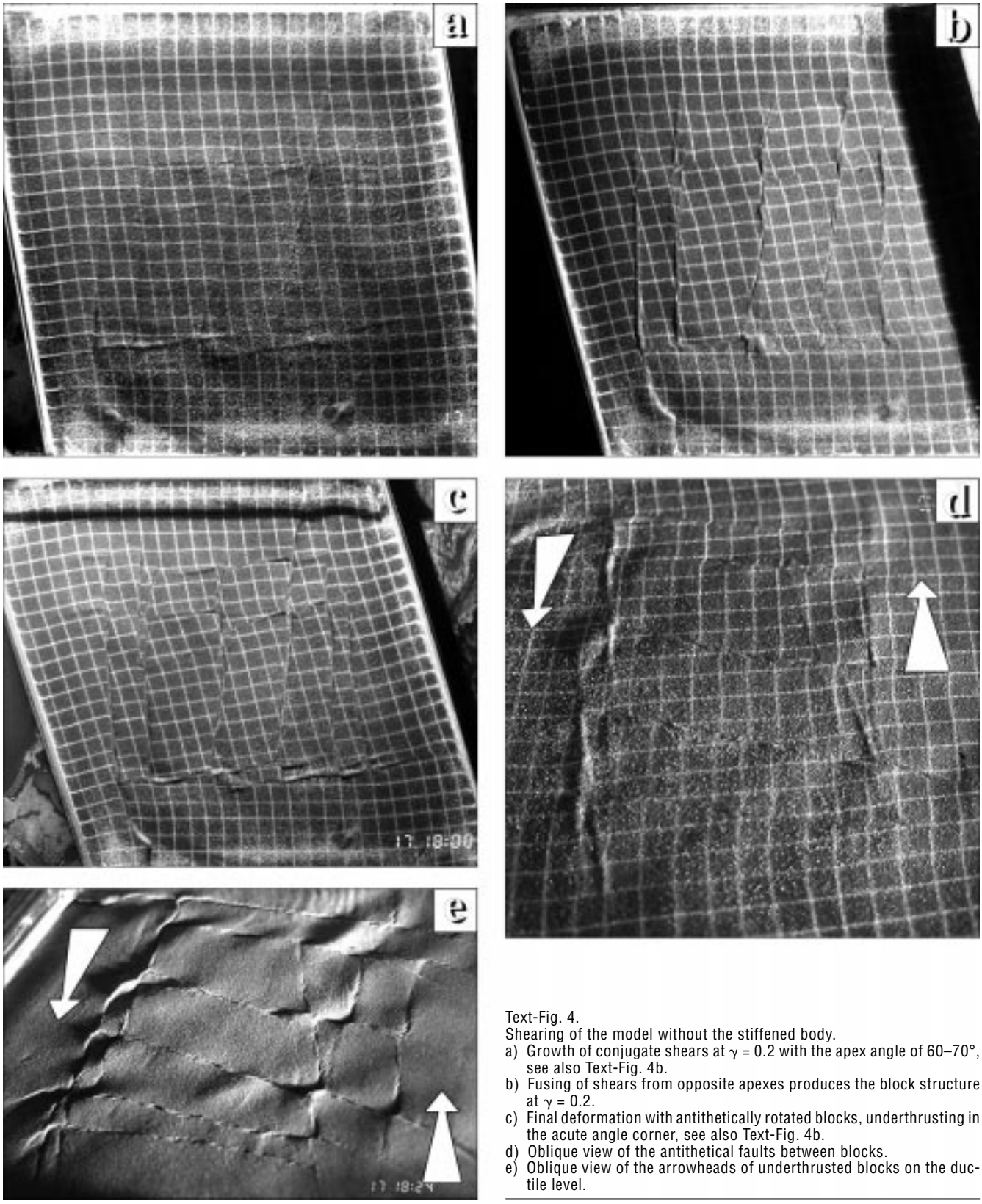

Text-Fig. 4.
Shearing of the model without the stiffened body.
a) Growth of conjugate shears at $\gamma = 0.2$ with the apex angle of 60–70°, see also Text-Fig. 4b.
b) Fusing of shears from opposite apexes produces the block structure at $\gamma = 0.2$.
c) Final deformation with antithetically rotated blocks, underthrusting in the acute angle corner, see also Text-Fig. 4b.
d) Oblique view of the antithetical faults between blocks.
e) Oblique view of the arrowheads of underthrusted blocks on the ductile level.

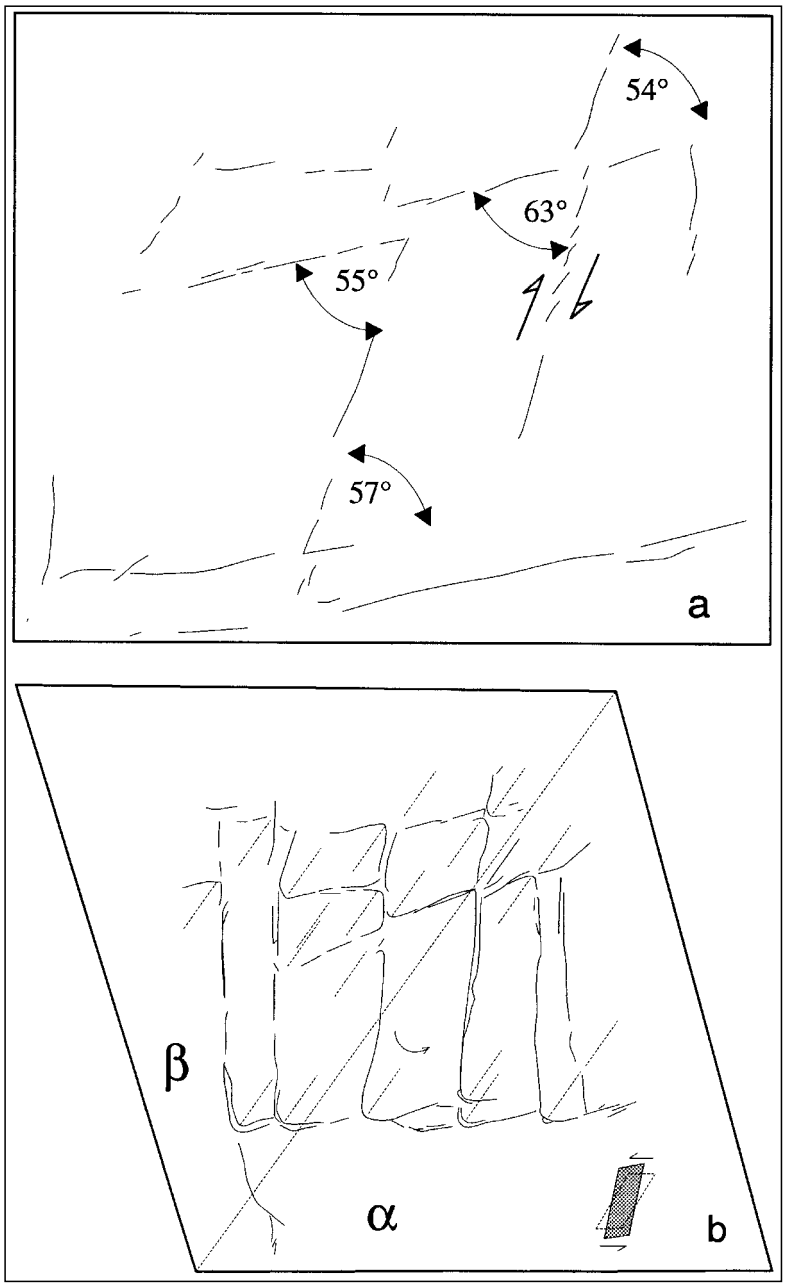

Text-Fig. 5.
a) Initial conjugate shears of the model, with the characteristic apex angle.
b) Final deformational aspect of experiment. The dashed lines provide the reference frame for measuring angles α and β.

2.3. Experimental Technique

We have run 11 experiments organized for:
1) the carriage and deficiency of the resistant bodies of the lithosphere dimensions,
2) the presence of two bodies and,
3) the variable lithosphere thermal situation-layering presuming cold (Archean) 4 rheological layers and hotter (late Variscan) 3-layers lithosphere.

We sheared selected models forward and backward.

We varied the size of the rotating part of the shear box walls in order to obtain model conditions for:
1) a narrow shear zone (10 cm) inside a larger lithosphere model (62 x 62 cm),
2) a broad bulk shear zone comprising the whole large lithospherical model (62 x 62 cm),
3) a bulk narrow shear zone comprising the whole lithospherical model (60 x 30 cm shear boxes).

3. Rheological Four-Layer Models

3.1. Wrenching of a Large, Cold "Lithospheric" Plate Without a Stiffened Body (Experiment 4.4)

These experiments supply the principal comprehension of the model behavior and assist for the comparison with trials with included stiffened body. Typical for this model is the late $\gamma = 0.2$ occurrence of conjugate shears. Their acute angle indicates and they are symmetric around the main stress axis. The conjugate shears developed with the opening angle of 55–60° (12 cm apart from walls, Text-Figs. 4 and 5a). The faults coalesced to form the lozenge-shaped uneven grid of parallel shear zones. The number of these fractures remained constant while new shears parallel to side walls occurred later in the experiment (Text-Fig. 4).

Rigid rotation of faults in the sense of the shear essentially incorporated the subsequent deformation. The border shears subparallel to the movement direction remained directionally stable while the oblique shears pivoted around the points of rotation in the centre of the model (Text-Fig. 5b). During the rotation of blocks their long axes migrate into the direction perpendicular to the shear zone boundaries and the arrowhead-like underthrusting occurred on the acute angle-restraining block corners (Text-Fig. 4d and 4e). The modifications of the initial angle (54°-55°) of the conjugate shears (Text-Fig. 5a) indicate the deformation of blocks and rotation (Text-Fig. 6).

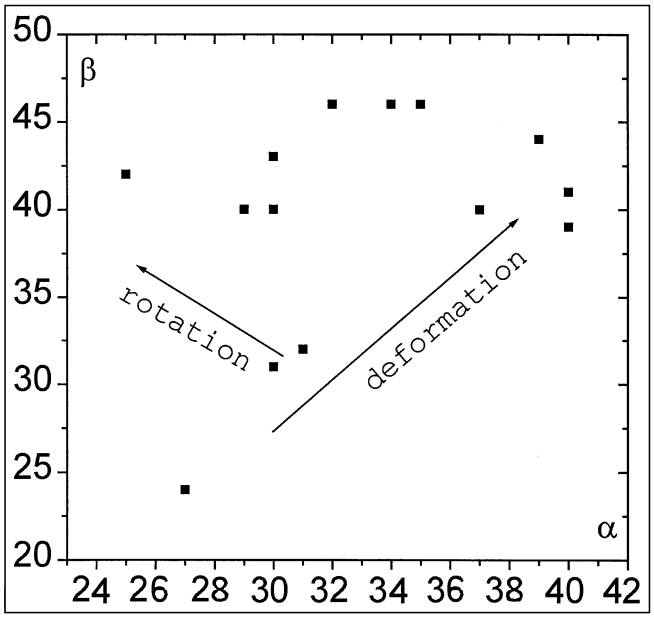

Text-Fig. 6.
Correlation graph of angles α and β that indicate either the deformation and/or rotation of the blocks with assumed constant initial conjugate shear angle.

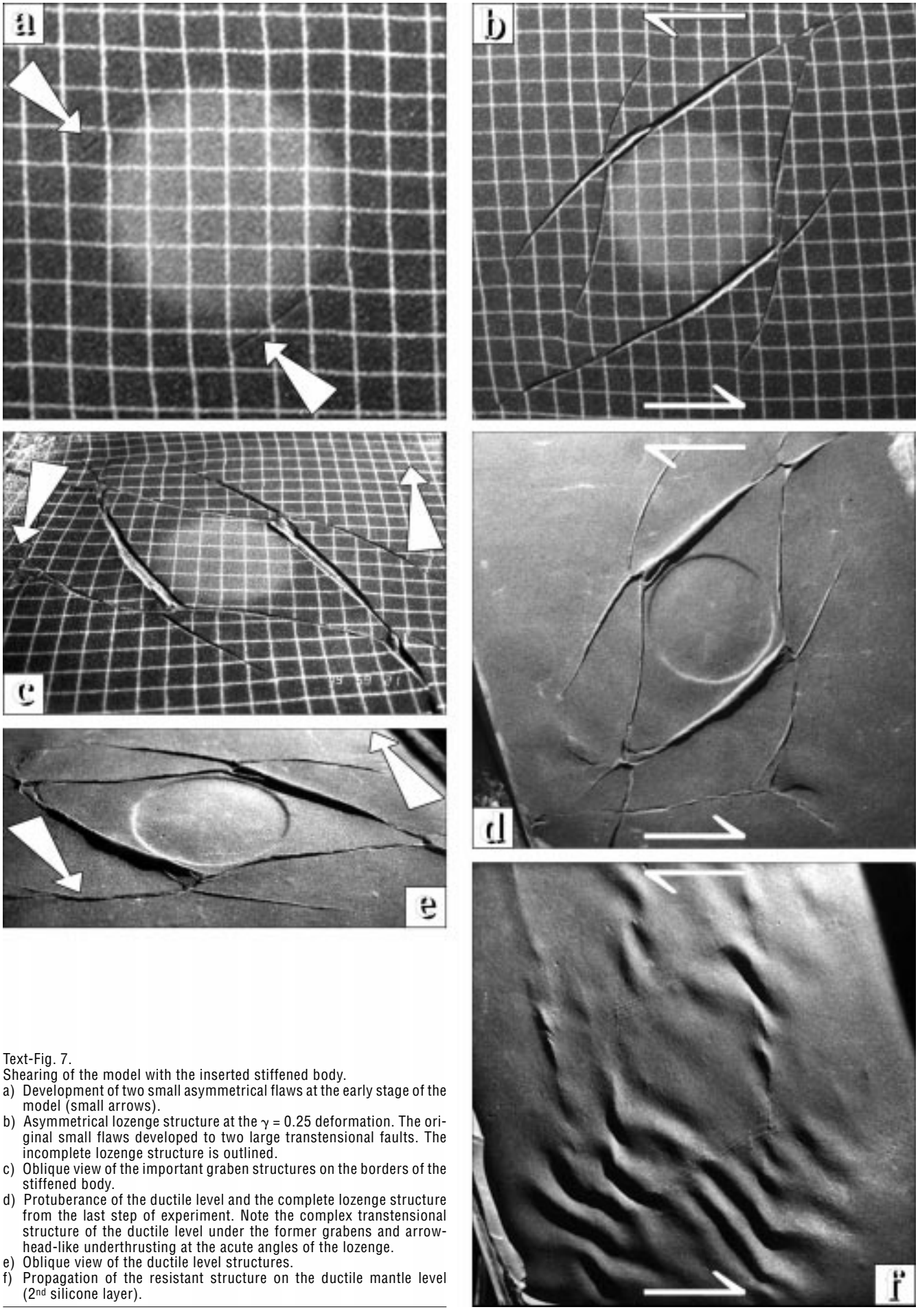

Text-Fig. 7.
Shearing of the model with the inserted stiffened body.
a) Development of two small asymmetrical flaws at the early stage of the model (small arrows).
b) Asymmetrical lozenge structure at the $\gamma = 0.25$ deformation. The original small flaws developed to two large transtensional faults. The incomplete lozenge structure is outlined.
c) Oblique view of the important graben structures on the borders of the stiffened body.
d) Protuberance of the ductile level and the complete lozenge structure from the last step of experiment. Note the complex transtensional structure of the ductile level under the former grabens and arrowhead-like underthrusting at the acute angles of the lozenge.
e) Oblique view of the ductile level structures.
f) Propagation of the resistant structure on the ductile mantle level (2nd silicone layer).

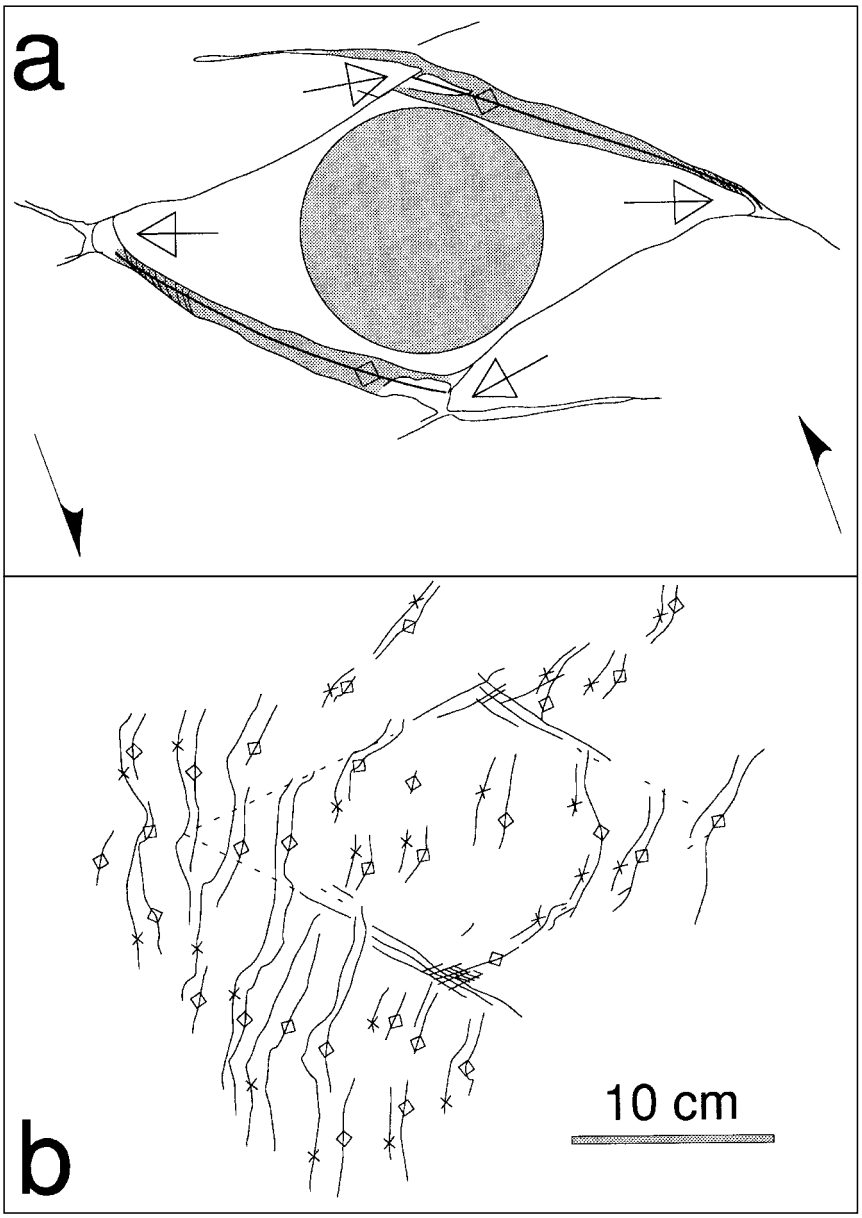

Text-Fig. 8.
Propagation of the deformation to the two ductile silicone layers.
a) Ductile crust layer.
b) Ductile mantle level.
Squared lines = anticlines; crosses = synclines; arrows = sense of the underthrusting in the acute lozenge corners.
Note the lesser folding inside the stiffened structure on the ductile mantle level.

3.2. Homogeneous Wrenching of a Large, Cold "Lithospheric" Plate with a Circular Stiffened Body (Experiment 4.2)

The resistant body of larger brittle crust thickness in the middle of the shear box had the following consequence:

1) It controls the premature propagation of the first shears,
2) the rotation and growth of unusual fractures in the proximity of the body,
3) the final fracture geometry is different.

Lesser rotation of the stiffened body in comparison with the rest of the model dominated from the beginning the strain pattern. This had for effect the early development of two flaws on the border of the resistant body (Text-Fig. 7a). After their initiation due to the slower rotation, significant transtension occurred along them. Other paired fractures appeared and successively developed, constructing with the early flaws a shear set with the apex opening angle about 40° (Text-Fig. 7b and d). They combined to lozenge structure. The faults bowed progressively during their propagation from the centre of the model alike to shears in the

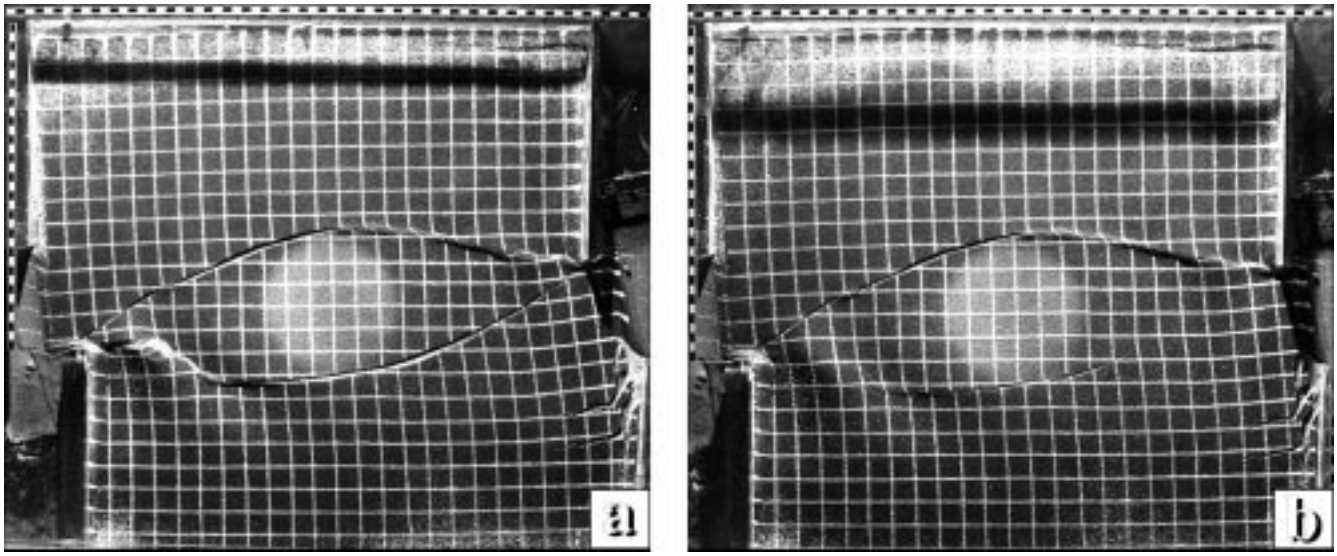

Text-Fig. 9.
Shearing of the large cold lithosphere with resistant body and narrow shear zone.
a) The final deformation after $\gamma = 0.5$. Grid spacing 2.5 cm.
b) One major fault that joins the two corners of the displacing container, second less developed shear occurs on the opposite border of the stiffened body.

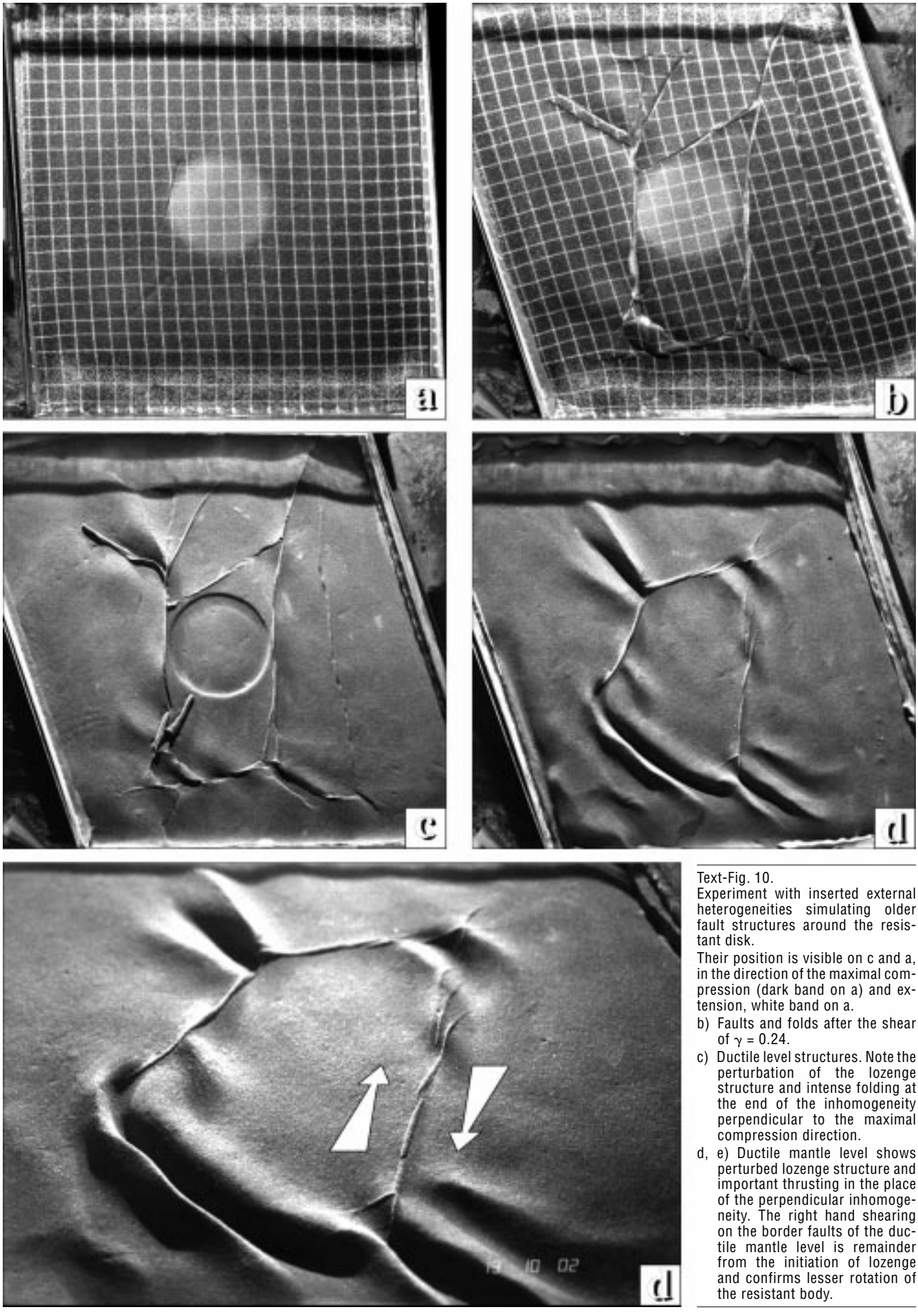

Text-Fig. 10.
Experiment with inserted external heterogeneities simulating older fault structures around the resistant disk.
Their position is visible on c and a, in the direction of the maximal compression (dark band on a) and extension, white band on a.

b) Faults and folds after the shear of $\gamma = 0.24$.

c) Ductile level structures. Note the perturbation of the lozenge structure and intense folding at the end of the inhomogeneity perpendicular to the maximal compression direction.

d, e) Ductile mantle level shows perturbed lozenge structure and important thrusting in the place of the perpendicular inhomogeneity. The right hand shearing on the border faults of the ductile mantle level is remainder from the initiation of lozenge and confirms lesser rotation of the resistant body.

shear zones (RAMSAY & HUBER, 1983). The final lozenge structure displays a distinctive asymmetry. The silicone protrusions of the "ductile crust" in place of the two main shears, that endured the larger part of the deformation, result from the spreading (extension) of fractures in the direction of the maximal stretching of the model (Text-Fig. 8).

3.3. Narrow Shear Zone in a Large, Cold "Lithospheric" Plate with a Circular Stiffened Body (Experiment 4.1)

In this experiment the shear box tolerated the 10 cm shear zone to develop inside the model (Text-Fig. 9). This shear zone is narrower than the stiffened body. The first flaw on the border of the rigid body developed in the direction of the main temporary stress axis exerted by two opposite moving sides of the box. It appeared at $\gamma = 0.25$ close to the moving wall. This fracture later joined quickly both opposite box corners (Text-Fig. 9b). It ripened into one single major shear zone. Only after this the other flaw appeared on the other side of the resistant circle and joined equally both opposite corners (Text-Fig. 9b). Strong folding perpendicular to the main stress orientation on the side of the moving corner emerged as the consequence of the unequally distributed strain through the model (Text-Fig. 9).

The result is a lens shaped edifice around the stiffened body and intense (up to the ductile mantle level) folding induced through the pinning of the lithosphere by the resistant disk (Text-Fig. 9).

3.4. Wrenching of a Large, Cold "Lithospheric" Plate with a Circular Stiffened Body Surrounded by Two Fault Zones (Experiment 4.3)

The silicone heterogeneities placed in the orientation of extension and compression axes imitated earlier faults (Text-Fig. 10). Fracture in the direction of maximal compression was closer to moving wall. The deformation brought on strong squeezing in the area of the inhomogeneity perpendicular to the main compression axis and extension across the fault parallel to the compression axis (Text-Fig. 10a).

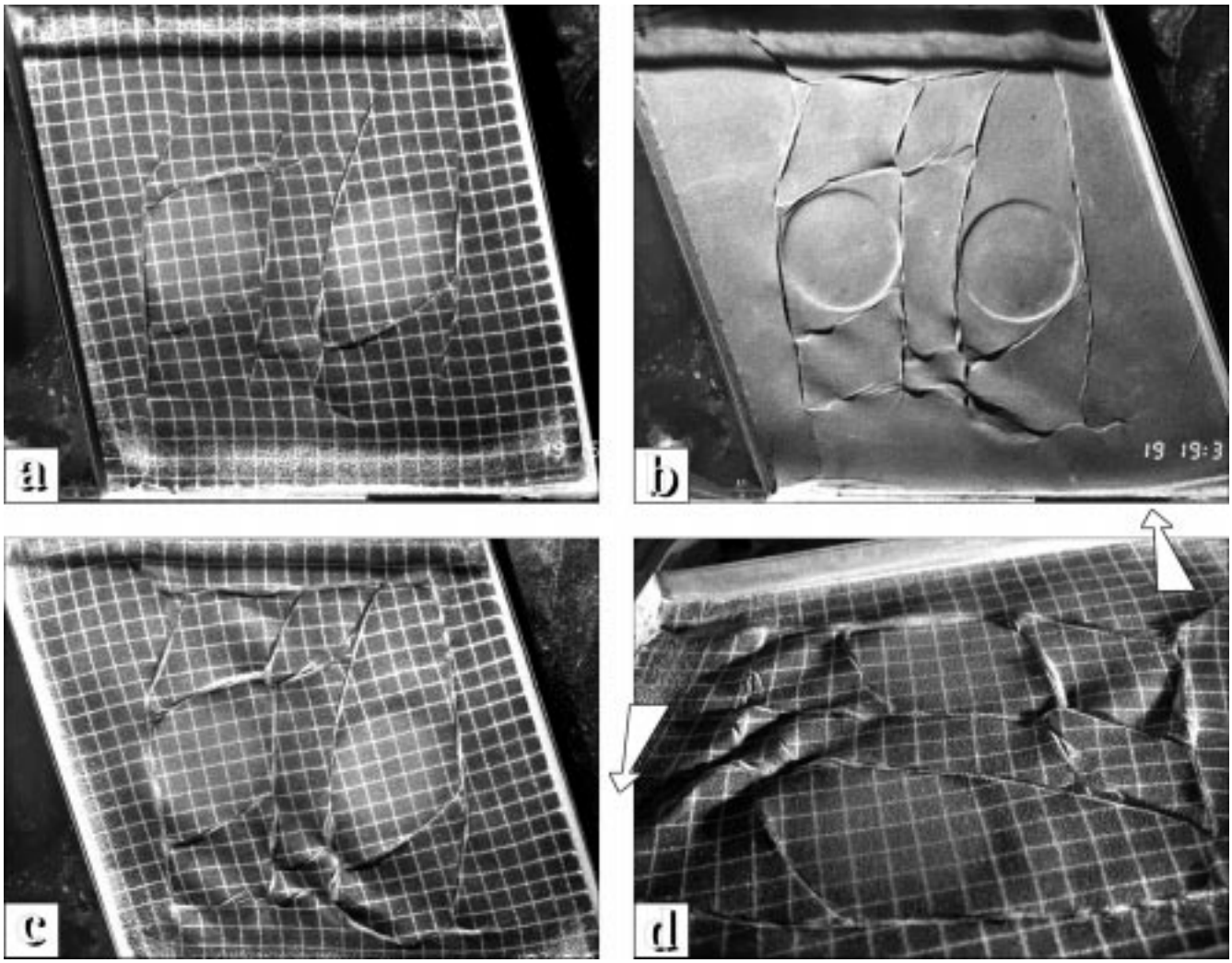

Text-Fig. 11.
Experiment with two inhomogeneities.
a) Deformational stage after the displacement of ($\gamma = 0.24$) shows complete development of the lozenge around the body closer to the moving corner of the shear box and the incomplete development around the remote body.
b) Final deformation of the ductile level shows strong folding close to the moving corner.
c) Strong folding in the area close to the moving corner of shear box.
d) Oblique view of the strong folding amplitude in the front of moving corner.

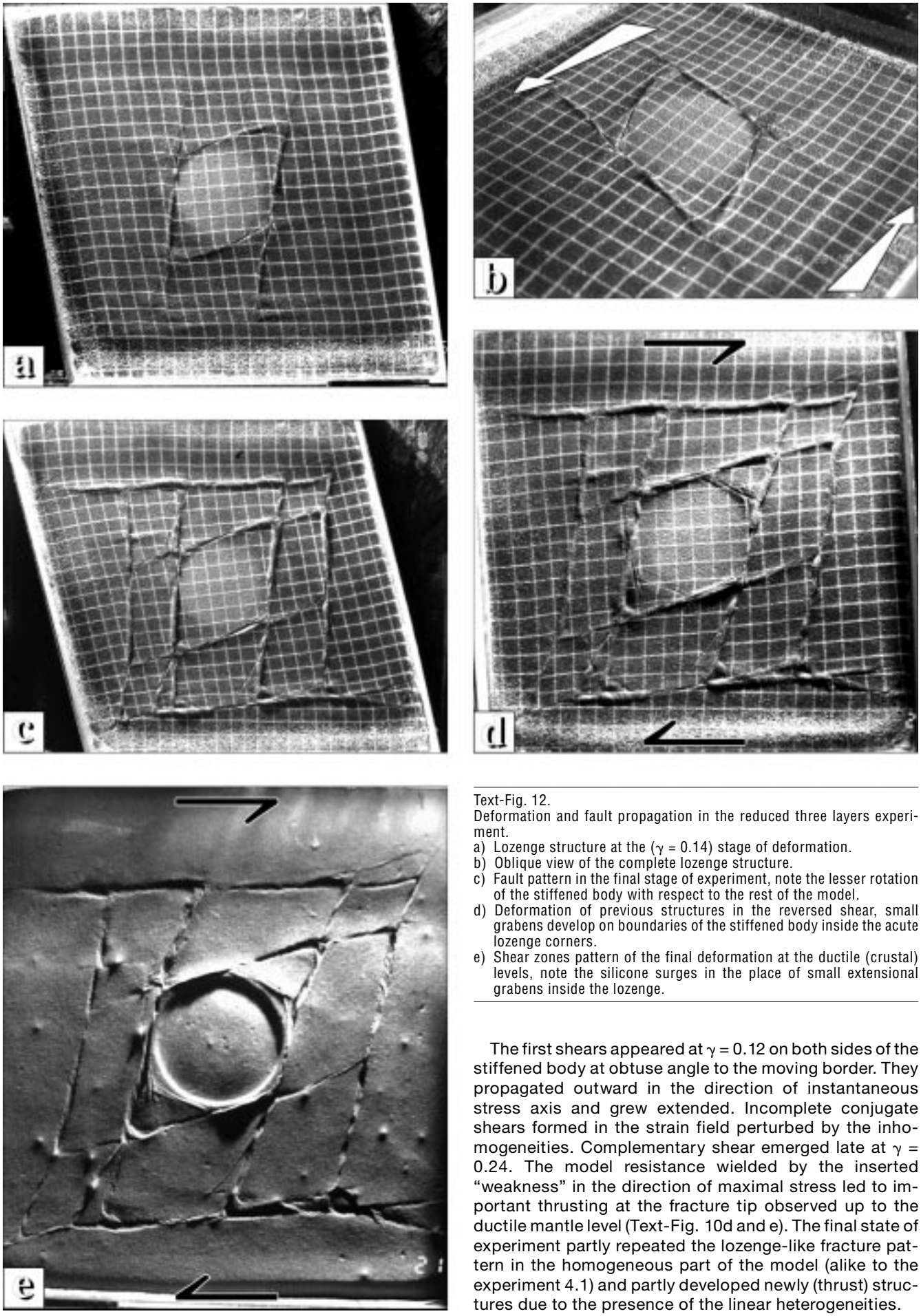

Text-Fig. 12.
Deformation and fault propagation in the reduced three layers experiment.
a) Lozenge structure at the (γ = 0.14) stage of deformation.
b) Oblique view of the complete lozenge structure.
c) Fault pattern in the final stage of experiment, note the lesser rotation of the stiffened body with respect to the rest of the model.
d) Deformation of previous structures in the reversed shear, small grabens develop on boundaries of the stiffened body inside the acute lozenge corners.
e) Shear zones pattern of the final deformation at the ductile (crustal) levels, note the silicone surges in the place of small extensional grabens inside the lozenge.

The first shears appeared at γ = 0.12 on both sides of the stiffened body at obtuse angle to the moving border. They propagated outward in the direction of instantaneous stress axis and grew extended. Incomplete conjugate shears formed in the strain field perturbed by the inhomogeneities. Complementary shear emerged late at γ = 0.24. The model resistance wielded by the inserted "weakness" in the direction of maximal stress led to important thrusting at the fracture tip observed up to the ductile mantle level (Text-Fig. 10d and e). The final state of experiment partly repeated the lozenge-like fracture pattern in the homogeneous part of the model (alike to the experiment 4.1) and partly developed newly (thrust) structures due to the presence of the linear heterogeneities.

3.5. Wrenching of a Large, Cold "Lithospheric" Plate with Two Circular Stiffened Bodies (Experiment 4.5)

The model included two resistant circular bodies, 7.5 cm apart (Text-Fig. 11). The first shears on both sides of the body closer to the moving corner occurred at $\gamma = .03$ and spread. Later at $\gamma = 0.1$, a complementary set of shears with the apex angles of 70° occurred in the proximity of the moving wall and on the opposite side of the first disk. At the final stage the periphery fracture formed on the edge of the fixed wall and allowed the rest of the model for rigid block rotation. The heterogeneous strain relocation in the model produced stronger folding on the side of the moving wall (Text-Fig. 11 c,d). It provoked equally the deficiency of shears on the opposite side of the second stiffened body. Striking folding and shear thrusting are visible in the ductile ("lower crust") position of the model (Text-Fig. 11b). It propagates down to the ductile mantle.

4. Rheological Three-Layer Models

4.1. Progressive and Inverted Wrenching of a Large, Hot Lithosphere with a Stiffened Body (Experiments 4.6 and 4.10)

The brittle "mantle" sand layer was absent. Only the upper (brittle) crust exerted the brittle strength in the model. Its thickness lowered correspondingly to 6 mm. The 3 mm of sand added to brittle crust shaped the stiffened body.

The first little conjugate shear set occurred at $\gamma = 0.06$ on the periphery of the stiffened body nearby the moving side. Together with the retarded shear from the other side of the resistant form they grew as symmetrical lozenge with the apex opening angle of 60° (Text-Fig. 12a and b). The shears at the periphery of the model (Text-Fig. 12c) sealed the inner fault system. The direction of later shears approached the direction of the conjugate shears but they mainly allowed inner blocks for rotation, separating them from the walls. At the end of the experiment new conjugate pairs of shears occurred with an apex angle of 45–50°.

Text-Fig. 13.
Detail of small strike-slip grabens from the acute corners of lozenge formed in the backward shear of the experiment 4.10.

We performed the shear sense reversal at the forward deformation of $\gamma_1 = 0.25$ and moved the shear box wall back. This led first to compression (inversion) across the fracture zones and to the formation of significant topographical heights. These zones took up nearly all the deformation up to $\gamma_2 = \gamma_1$. At this phase, new small extensional faults developed at the boundary of the stiffened body. They consist of two straight offset parts, slightly curved at their junction (Text-Fig. 12d and e, Text-Fig. 13). The perimeter of the lozenge surrounding the resistant form constrains this set of fractures. They spread later to the new regular pattern of parallel shears (RIEDEL shears) at 30° angle to the moving wall. They are distributed through the whole model but confined between the faults from the forward run.

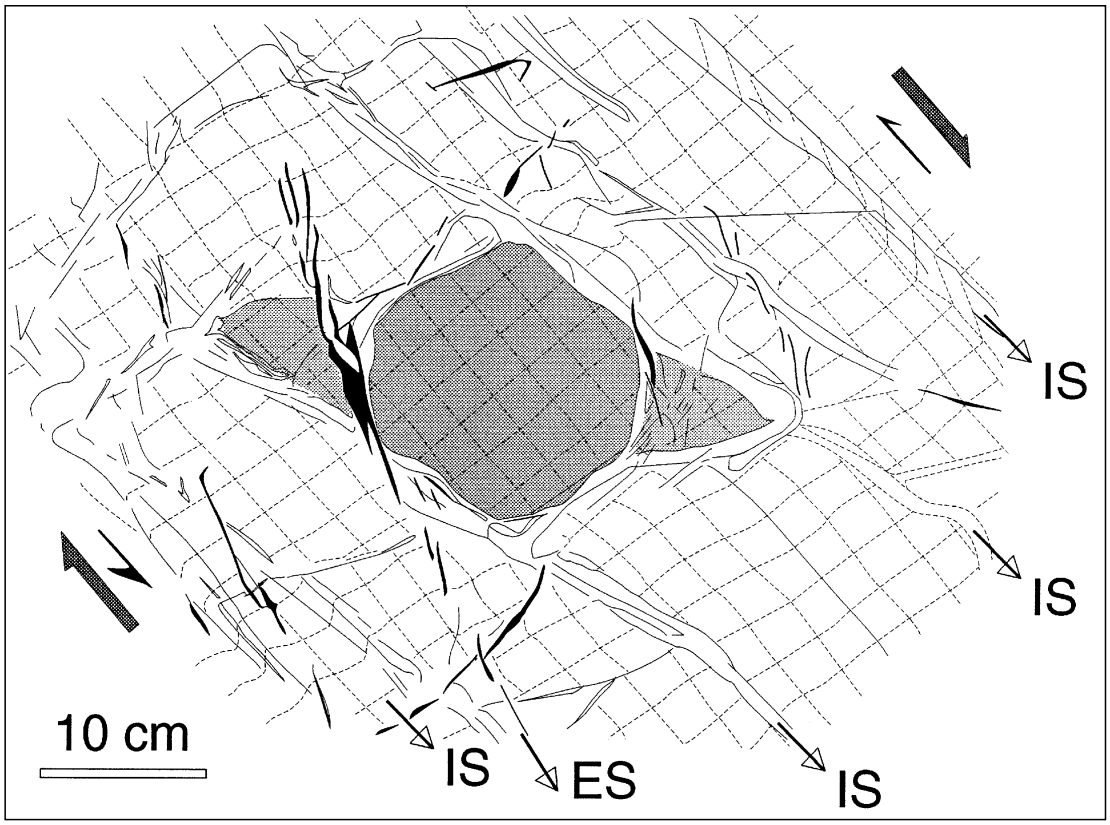

Text-Fig. 14.
Ductile deformation of the lozenge structure together with the previous fault pattern in the backward shear.
ES = extension shears; IS = inversion structures; hatched lines = marker grid of the experiment.

Ductile deformation of the earlier lozenge structure around the stiffened body appeared. New shears distinctly dissect and offset it on the side closer to the moving wall side (Text-Fig. 13 and 14). The ductile crust traces particularly the deformation of the lozenge. An identical fracture pattern arose from the second repetition of the experiment (Experiment 4.10). In order to surmount the resistance of the model lithosphere hardened with earlier fractures a double speed of 14 cm per hour drove the movement reversal.

4.2. Wrenching of a Large, Hot "Lithospheric" Plate with a Stiffened Body Containing Inner Zones of Weakness (Experiment 4.7)

The stiffened body contained two zones of weakness. They imitated a set of older faults. We have chosen one fracture parallel to the main extension axis and the second perpendicular to it. Concentrated compression occurred across the fault perpendicular to main compression axis and extension across the perpendicular (Text-Fig. 15a). A conjugate shear set with high apex angle of 80° developed tightly on the edge of the body producing larger shear zones. At the end of the experiment the conjugate shears with the apex angle of 40° appeared. Strong folding and thrusting emerged at the stiffened body rim in the places where we have introduced the zone of weakness.

New small faults on the periphery of the circular body enclosed in the lozenge came into view, in the reversed shear similarly to the other reversed experiments (Text-Fig. 15).

5. Experiments with a Narrow Shear Zone

5.1. Progressive and Reverse Wrenching of a Cold "Lithospheric" Plate with a Stiffened Body (Experiment 4.8)

We drove the experiment with the increased speed of 12 cm per hour. The narrow size of the shear zone had for consequence strong folding around the resistant circle in the edge of moving piston (Text-Fig. 16a). The deforma-

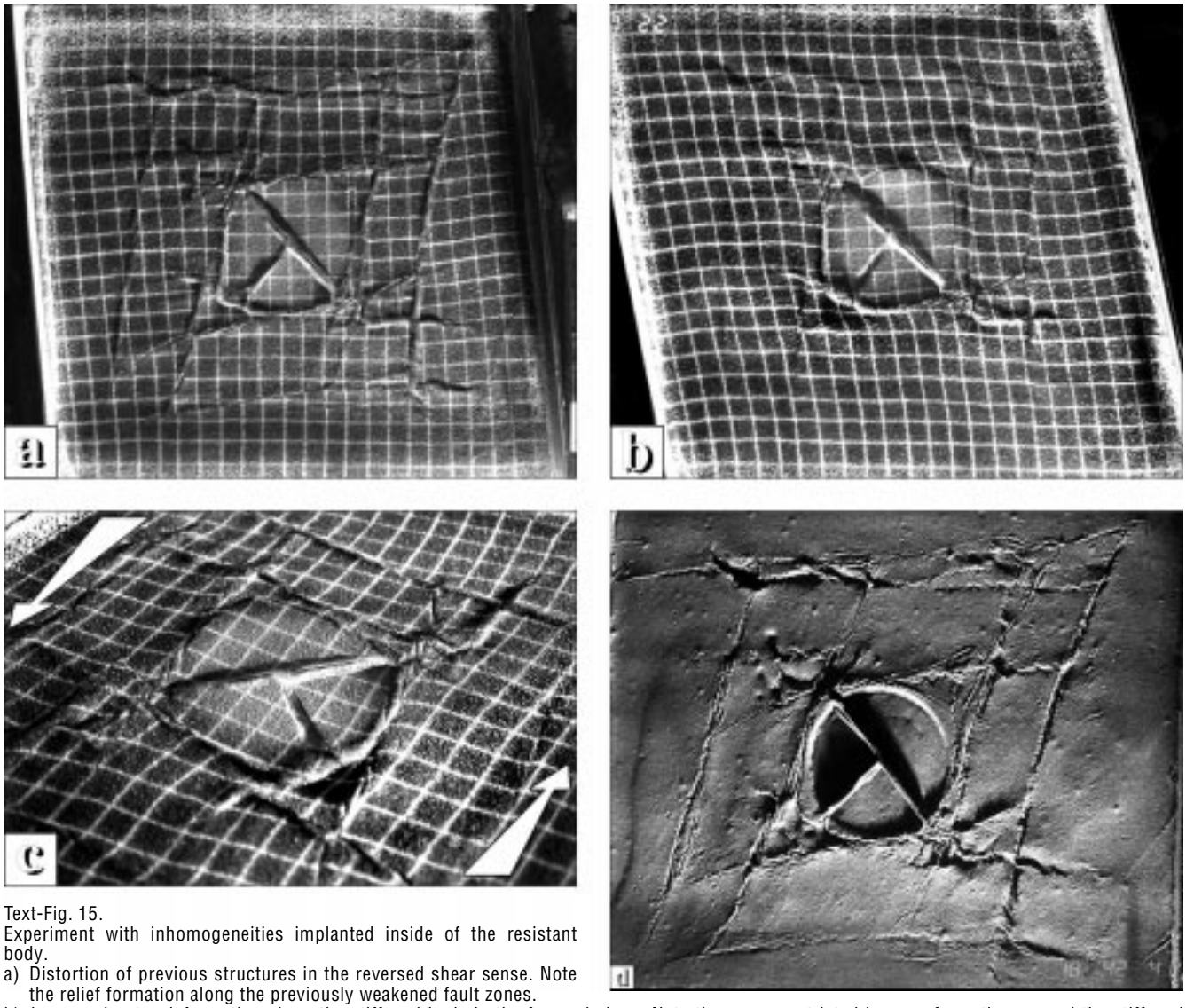

Text-Fig. 15.
Experiment with inhomogeneities implanted inside of the resistant body.
a) Distortion of previous structures in the reversed shear sense. Note the relief formation along the previously weakened fault zones.
b) Inner and outer deformation along the stiffened body in the forward shear. Note the very constricted lozenge formation around the stiffened body.
c) Oblique view of the structure in the backward shearing.
d) Ductile crust – first silicone level in the final strain state after the backward shearing.

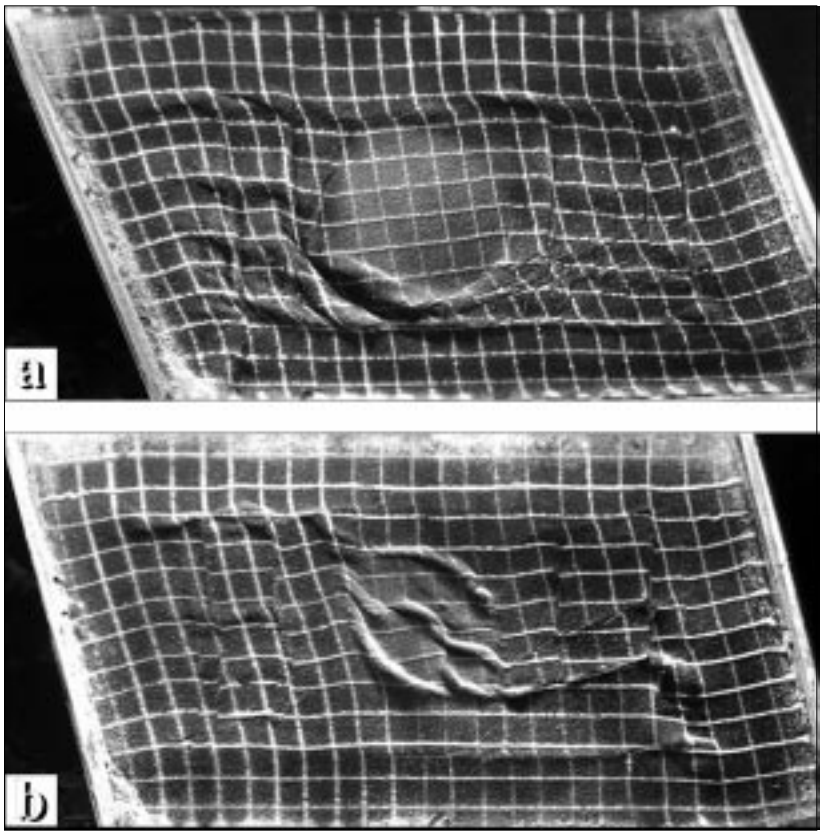

Text-Fig. 16.
Deformation of the resistant body in the narrow shear zone.
a) 3-layer model (without the sand layer representing the brittle crust). Note the almost absent development of the surrounding lozenge of the stiffened structure.
b) Model with the inserted stiffened body at the brittle mantle level and with the correspondingly lowered thickness of brittle crust. Note the strong inner deformation (folding) of the surface above the rigid body.

tion of the model concentrated between the bordering major fractures. Distributed small conjugate shear sets with the apex angle of 60–65° developed behind the body. Faint contour of the suppressed lozenge structure is still detectable (Text-Figs. 16a and 18 g).

5.2. Wrenching of a Hot Lithosphere with a Stiffened Body on the Level of the Brittle Mantle (Experiment 4.9)

In this experiment the presence of a rigid body in some deeper parts of the lithosphere, with the protrusion of the ductile crust and with the reduced thickness of the upper brittle crust was modelled. The surroundings of the body were built of three layers: two layers of silicone and 8 millimeters of sand as brittle crust. The 8 millimeters stratum of the sand between the two silicone layers fashioned the stiffened body.

Strong folding due to reduced strength of the cap occurred inside and on the borders of the resistant body. Conjugate shears of the apex angle of 30° evolved in the same time and later in the deformation. The lozenge structure is missing.

6. Discussion

The lozenge form of blocks evolved from the conjugate shears around the stiffened body, located in the brittle crust and it is the typical feature ensuing from the presence of the rigid body in the deformed lithosphere (Text-Fig. 17 and 18). The apex angles of lozenges vary following to various factors, but mainly with the total thickness of sand in the experiments. The angles are higher for the reduced sand thicknesses. They reflect the basic COULOMB behavior of the model.

During the experiments we couldn't avoid the border effect – formation of fractures on the model margin owing to cohesion between sand and the stretching gum walls. This is visible on the preserved, undeformed internal net of the blocks adjacent to the box walls. Because the faults in all cases propagated mostly from the centre of the model, this effect influenced only the areas close to the stretching walls.

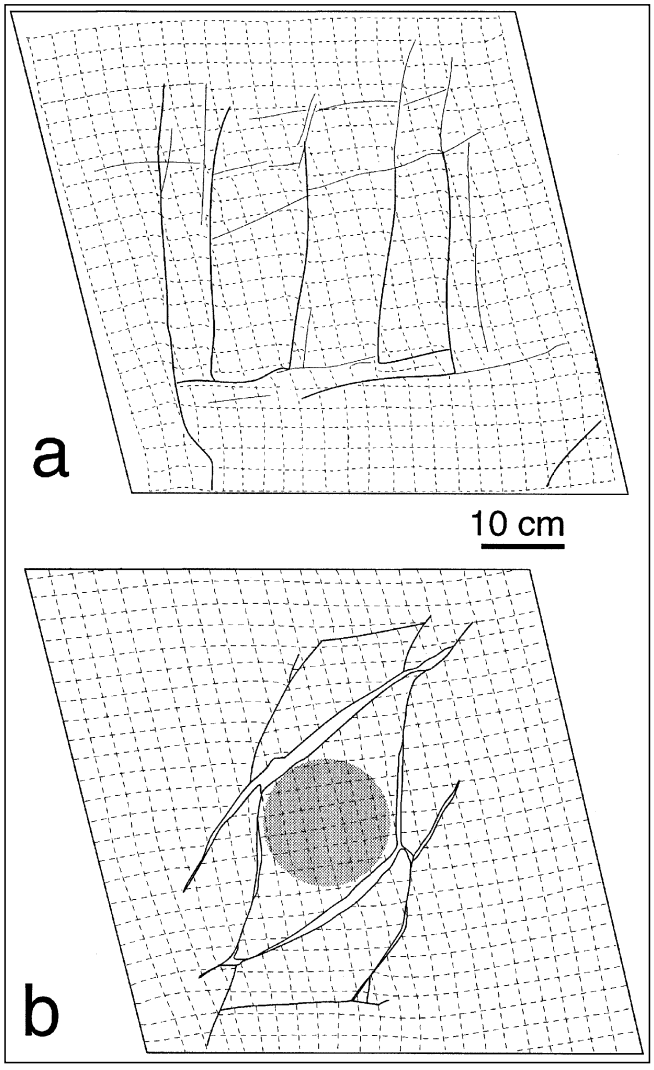

Text-Fig. 17.
Comparison of the models representing
a) the homogeneous plate and
b) the plate with the stiffened body.

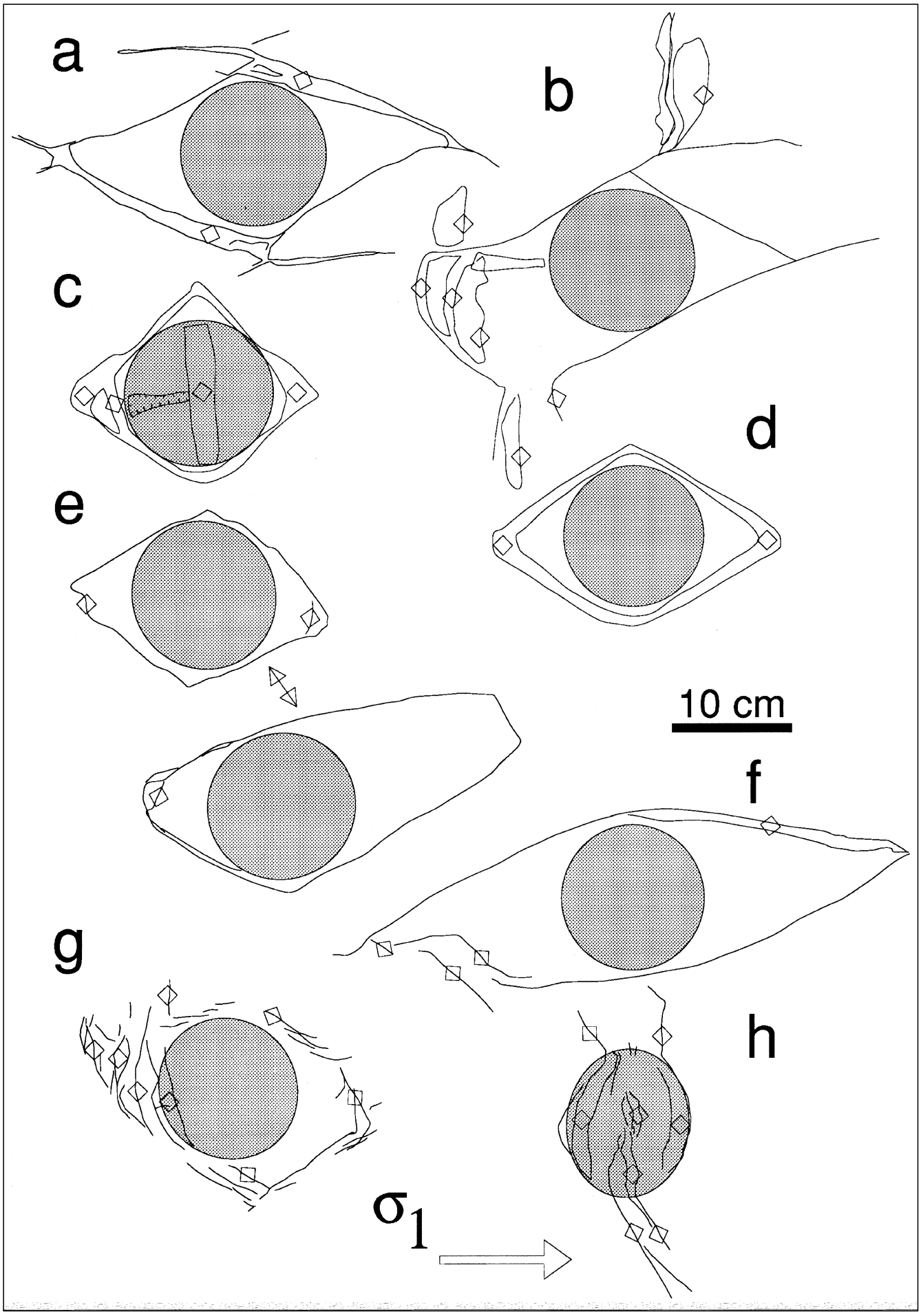
a
b
c
d
e
f
g
h
10 cm
σ1

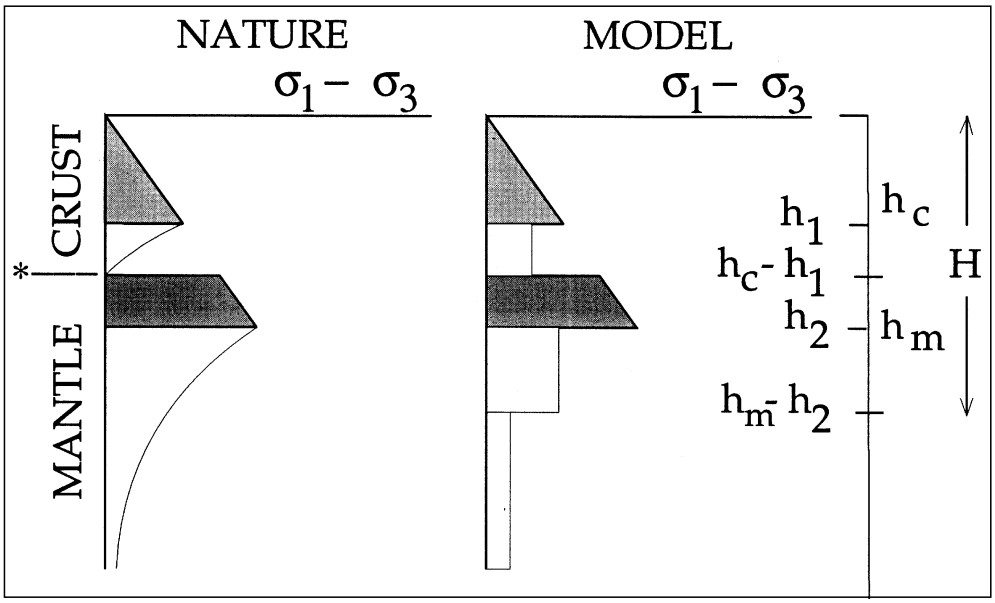

Text-Fig. 19.
Model rheological profile of the lithosphere and scaling with the materials used in experiments.
white: ductile levels in the nature and in the experiments; grey: brittle layers.

7. Summary and Conclusions

The propagation of conjugate shears with the apex angle mostly around 60° for the the hot lithosphere and 30° for the cold lithosphere provided the basic deformational feature of the models studied. The conjugate shear that appears at $\gamma = 0.1$ in models without a stiffened body, cracked the brittle crust into blocks (Text-Fig. 17a).

The fractures remained straight and only slightly curved or bent. The larger part of later deformation embodied the rotation of blocks and ductile deformation in the narrow shear zones along the block borders. The attitude of blocks in the strain field initiates the arrow-like underthrusting of the acute-restraining angle corners and transtension at the obtuse-releasing corners.

The stiffened body rotated more slowly than the remainder of the model during the first increments of deformation. As a consequence symmetrical flaws first localize (at $\gamma = 0.03$) at the borders of the rigid structure. They extend rapidly into pivoting faults of the transtensional and transpresssional type and later – in the 4 layer models – into prominent graben structures. At a later phase, as in the experiments without the rigid body, conjugate shears developed. The wrenched and reactivated lithosphere reveals thus the unyielding portions.

The final pattern of all experiments is a lozenge-like block fragmentation. Inserted additional heterogeneity into the model hardened the corresponding portion of the model and induced the lithosphere thrusting.

Our experiments suggest that the lozenge form of crustal blocks can help by kinematical reconstructions. The lozenge indicates the stress field. After its initiation it spins with the acute angle apex into the direction of maximum stress. This occurred in all our experiments. The deformed blocks change the original apex angle but if the asymmetry remains preserved, it indicates the orientation of the stress field prevailing at the time of the first conjugate shear development.

The shear sense reversal provided the closest fit of models with the fracture system in the Bohemian Massif. We obtained the grabens comparable to Permian basins from the eastern part of the Massif in the restraining corners of the enveloping lozenges.

Appendix

The model for the rheologic response of the lithosphere simplifies to the curve of one or two brittle layers (Text-Fig. 3 and 19) (RANALLI & MURPHY, 1987; DAVY & COBBOLD, 1988, 1991). Assuming that

h_1 = thickness of the brittle crust in meters,
h_c = total thickness of the crust,
$h_c - h_1$ = ductile crust,
$h_2 - h_1$ = thickness of brittle mantle,
$h_m - h_2$ = thickness of ductile mantle,
ρ_1 = density of the crust kg/m,
ρ_2 = density of mantle in kg/m,
μ_1 = viscosity of the ductile crust,
μ_2 = viscosity of the ductile mantle, and
g = gravity acceleration ($m.s^{-1}$)

the deviatoric stress at the base of the first brittle layer

$$\sigma bc = \tfrac{2}{3}\, \rho_1 \cdot g \cdot h_1 , \qquad (5)$$

and similarly for the deviatoric stress inside of the 1st silicone is

$$\sigma dc = \mu_1 \cdot \varepsilon,$$

where

$$\varepsilon = \text{velocity of piston/x} \qquad (6)$$

Text-Fig. 18. ◀◁◀
Summary of shapes of lozenge structures developed in the models.
a) 4-layered lithosphere.
b) 4-layered lithosphere with the external heterogeneity surrounding the stiffened structure.
c) 3-layered lithosphere with inhomogeneities inserted into the resistant structure.
d) 3-layered lithosphere.
e) 3-layered lithosphere with two stiffened bodies.
f) Large 4-layered lithosphere with the narrow shear zone.
g) Narrow shear zone in 4 layered lithosphere.
h) Resistant body on the brittle mantle level in the 3-layered lithosphere and in the narrow shear zone scene.
Squared lines = anticlines and/or inversion structures.

x = characteristic thickness of the model and length of the model and similarly for the second silicone.

The deviatoric stress inside of the 2nd silicone is

$$\sigma dm = \mu_2 \cdot \varepsilon, \quad (7)$$

and the deviatoric stress on the top of the second sand (mantle) layer is calculated as

$$\sigma bc = {}^2/_3\ \rho_2 \cdot g \cdot h_c, \quad (8)$$

where h_c = total thickness of the brittle crust. The total strength of the first sand layer is the area of the envelope of the deviatoric stress curve or the integral

$$F_1 = {}_0\int^{h_1} {}^2/_3\ \rho_1\, g dz, \quad (9)$$

and the strength of the second silicon layer

$$F_2 = {}_h\int^{H} \mu_2\, \varepsilon dz, \quad (10)$$

where H = total thickness of the lithosphere.

Acknowledgements

T. ENGELDER and R. KRANTZ offered advice and criticism on an early draft of this study. T. ENGELDER helped considerably to improve the English and clarify the text.

References

BENEK, R.: Aspects of late-Variscan strike-slip movements in northern Central Europe. – 1st International Conference on the Bohemian Massif, Prague, 26, Oct. 3, 1988, Czech Geological Survey, 15–18, 1988.

CHARDON, D.: Approche mécanique des déformations gravitaires de la protocroute continentale archéenne. – Geosciences Rennes 1993.

COBBOLD, P.R. & JACKSON, M.P.A.: Gum rosin (colophony): a suitable material for thermomechanical modelling of the lithosphere. – Tectonophysics, **210**, 255–271, 1992.

COBBOLD, P.R., DAVY, P., GAPAIS, D., ROSSELLO, E.A., SADYBAKASOV, E., THOMAS, J.C., TONDJII BIYO, J.J. & URREZTIETTA, M., DE: Sedimentary basins and crustal thickening. – Sedimentary Geology, **86**, 77–89, 1993.

DAVY, P. & COBBOLD, P.R.: Indentation tectonics in nature and experiment – 1. Experiments scaled for gravity. – Bull. Geol. Inst. Uppsala, N.S., **14**, 129–141, 1988.

DAVY, P. & COBBOLD, P.R.: Experiments on shortening of a 4-layer model of the continental lithosphere. – Tectonophysics, **188**, 1–25, 1991.

ENGLAND, P. & HOUSEMAN, G.: Role of lithospheric strength heterogeneities in the tectonics of Tibet and neighbouring regions. – Nature, **315**, 297–301, 1985.

GALAGHER, J.: Tectonics of China: continental scale cataclastic flow. – In: N.L. CARTER FRIEDMAN, M., LOGAN, J.M. & STEARNS, D.W. (Eds): Mechanical behavior of crustal rocks, Am. Geophys. Union, Washington, 259–273, 1981.

HOLMES: Physical geology. – 1–1288 (Nelson & Sons) London 1967.

KOSSMAT, F.: Gliederung des variszischen Gebirgsbaus. – Abh. Sachs. geol. Landesamt, **1**, 1–39, 1927.

KRANTZ, R.W.: Measurements of friction coefficients and cohesion for faulting and fault reactivation in laboratory models using sand and sand mixtures. – Tectonophysics, **188**, 230–207, 1991.

MOLNAR, P. & TAPPONNIER, P.: A possible dependence of tectonic strength on the age of the crust in Asia. – Earth Planet. Sci. Letters, **52**, 107–114, 1981.

NORMAN, J.W.: Tectonic effects of old very large meteoritic impacts on Earth showing on satellite imagery: a review and speculations. – J. Struct. Geol., **6**, 737–747, 1984.

POROSHIN, S.V.: Ring structures based on interpreting satellite photographs. – Int. geol. Rev., **23**, 1373–1378, 1981.

RAJLICH, P.: Circular and lozenge structure of the Bohemian Massif. – Jb. Geol. B.-A., **137/4**, Wien 1995.

RAMSAY, J.G. & HUBER, M.I.: The techniques of modern structural geology, Vol. I, Strain analysis. – London 1983.

RANALLI, G. & MURPHY, D.C.: Rheological stratification of the lithosphere. – Tectonophysics, **132**, 281–295, 1987.

RICHARD, P. & KRANTZ, R.W.: Experiment on fault reactivation in strike-slip mode. – Tectonophysics, **188**, 117–131, 1991.

SAOUL, J.M.: Circular structures of large scale and great age on the Earth's crust. – Nature, **271**, 345–349, 1978.

SCHTCHEGLOV, A.D.: Metallogeny of median masses. – Nedra, Moscow, 1–148, 1971.

SUESS, E.: Das Antlitz der Erde. – Wien (Tempsky) 1885, 1888, 1901, 1909.

VACEK, J., CHLUPÁC, I. & KLOMINSKÝ, J.: Stratigraphy of the Czech Republic (Geol. Survey Prague). – Unpublished report, 1988.

VENDEVILLE, B., COBBOLD, P.R., DAVY, P., BRUN, J.P. & CHOUKROUNE, P.: Physical models of extensional tectonics at various scales. – Continental Extensional Tectonics, London, Geol. Soc. London Spec. Publ., 95–107, 1987.

VILOTTE, J.P., DAIGNIERS, M., MADARIAGA, R. & ZIENKIEWICZ, O.C.: The role of a heterogeneous inclusion during continental collision. – Phys. Earth Planet. Int., **36**, 236–259, 1984.

WEIJERMARS, R. & SCHMELING, H.: Scaling of newtonian and non-newtonian fluid dynamics without inertia for quantitative modelling of rock flow due to gravity (including the concept of rheological similarity). – Phys. Earth. Planet. Int., **43**, 316–330, 1986.

WILLIAMS, H.: Tectonic lithofacies map of the Appalachian orogen. – Memorial University of Newfoundland, St John's NFLD, 1978.

Manuskript bei der Schriftleitung eingelangt am 7. Mai 1996